ISSN 2959-6157

An Optimized Hybrid ARIMA-GARCH Model Application on RR Interval Time Series Prediction for Heart Disease

Sicheng Shu[1,*]

Jinan University-University of Birmingham Joint Institute (J-BJI),
Jinan University, Guangzhou, China
*Corresponding author: sxs1934@student.bham.ac.uk

Abstract:

Heart disease is one of the highest mortality rate diseases worldwide, with arrhythmias frequently serving as a trigger (such as cardiomyopathy) or a complication (such as coronary heart disease) for cardiovascular diseases. Therefore, it is crucial to monitor abnormalities in heart function through the early identification of deviations in heart rate variability (HRV). In modern medical systems, wearable real-time monitoring devices and artificial intelligence are commonly employed to generate electrocardiograms (ECGs) and analyze HRV data. The key to this application lies in making reasonable judgments of HRV data using data mining tools, including multiple linear regression, support vector machine, random forest, or long-short-term memory neural networks. However, these models fail to yield satisfactory results for cardiac rhythm monitoring. Consequently, the paper introduces an optimized hybrid ARIMA-GARCH model to enable heart disease detection and pathological diagnosis, playing a guiding role in personalized treatment and the tracking of the cardiovascular health status of monitored individuals. The proposed model combines data preprocessing using the one-sided Hodrick Prescott filter and parameter tuning based on partitioning-interpolation techniques and Fast Discrete Fourier Transform to fit and predict the RR interval time series. Experimental results indicate that our proposed model exhibits significant advantages in quantitative assessments compared to other models, as it effectively preserves the trend and accounts for high volatility in short-term forward prediction.

Keywords: optimized hybrid ARIMA-GARCH model; RR interval time series prediction; cardiac rhythm monitoring.

1. Introduction

According to the World Health Organization (WHO), heart diseases, also known as cardiovascular diseases (CDs) in medical terminology, are estimated to claim the lives of 17.9 million people annually. CDs encompass a range of conditions affecting the heart and blood vessels, including coronary heart disease, rheumatic heart disease, and other related disorders[1]. Heart rate, one of the primary indicators of cardiac health, is the number of times the heart contracts and relaxes to pump blood within a given time frame, typically one minute, with an average resting range of 60-80 beats [1]. Early detection of arrhythmias is beneficial for the preliminary diagnosis of CDs, contributing doctors to developing personalized treatment plans and playing a crucial role in inhibiting the progression of these conditions [1, 2].

Clinically, multi-lead electrocardiogram (ECG) systems are commonly used to measure the temporal variations in heart rate [3]. This variability is defined as the changes in the time intervals between successive heartbeats, known as heart rate variability (HRV) [4]. The most frequently used metric is the RR interval, the time interval between adjacent R waves in the ECG signal. HRV is primarily controlled by the interaction between the autonomic nervous system (ANS) and receptors in the sinoatrial node (SAN), influenced by multiple factors such as exercise, emotion, circadian rhythms, hormonal regulation, and neural modulation. It exhibits complex behavior in the time domain, with significant differences in data characteristics among individuals of varying ages, genders, and health statuses [5, 6, 7]. These complexities have limited the utility of fixed, multi-operator-required ECG devices for essential monitoring across a broad population. However, with advancements in technologies such as artificial intelligence (AI) and sensors, single-lead ECG systems

1 https://www.who.int/health-topics/cardiovascular-diseases/#tab=tab_1

can be integrated into wearable, real-time monitoring devices, serving as a promising alternative to multi-lead ECG systems. Nevertheless, this technology's challenges, such as motion artifacts, pose significant hurdles [3].

In recent years, emerging machine learning techniques have been widely applied to predicting, verifying, and revising HRV data. Furthermore, from a broader academic perspective, time-domain characteristics of HRV can also be analyzed using time series analysis models from econometrics as predictive tools to achieve the medical practical purposes mentioned earlier. However, models have yet to emerge singly capable of exhibiting robust generalization across diverse datasets.

To solve this problem, the paper embraces the paradigm of integrating the advantages of distinct models to overcome their deficiencies, thereby directing our focus toward hybrid modeling approaches. Drawing on references [8], [9], and [10], the paper proposes an optimized hybrid ARIMA-GARCH model. This model exhibits strong generalization capabilities across various datasets and has surpassed the limitations of previous models regarding prediction accuracy. These advantages mitigate the instability associated with heart rhythm monitoring across diverse groups. And it facilitates advancements in the prevention and treatment methods for heart diseases.

The proposed model initially utilizes the one-sided Hodrick Prescott (HP-1s) filter to decompose the logarithmically transformed raw data into a sum of segments with high trend and low volatility (linear part) and segments with low trend and high volatility (nonlinear part). In addressing the linear component of the dataset, the proposed hybrid model forthrightly adopts the ARIMA methodology for curve fitting and generating forecasts. Meanwhile, for the nonlinear segment, marked by minimal trend and considerable volatility, the model initiates the analytical process by implementing a partitioning strategy that discretizes the dataset into multiple subsets. In adherence to the Nyquist Sampling Theorem, the model employs the Fast Discrete Fourier Transform (FDFT) to transmute the discrete data points into a continuous waveform. This transformation facilitates the construction of a spectral plot, through which the model identifies the peak frequency of the signal, culminating in the determination of an appropriate sampling step size. After that, the model employs interpolative techniques to augment the data point count within each subset, ensuring that each partition is adequately represented. Subsequently, each subset is independently subjected to the GARCH model fitting procedure, yielding the optimal GARCH model for every partition. It is subsequently applied to the aggregate dataset for retrospective prediction. The ultimate forecasted outcomes are synthesized by integrating the projections furnished by the ARIMA model with the optimal GARCH model.

The remainder of this paper is structured as follows. Section II provides a comprehensive review of the related methods and models found in the literature. Section III elaborates on the principles and the specific implementation process of the optimized ARIMA-GARCH hybrid model. Section III discusses the quantitative analysis of the model's performance on the test set and a comparison with traditional models. Finally, Section IV concludes the paper.

2. Related Work

A comprehensive study in [1] compared the predictive capabilities of methods such as ARIMA models, linear regression, support vector machines (SVM), k-nearest neighbors (KNN), decision trees, random forests, and long short-term memory neural networks (LSTM) for multistep forward prediction of heart rate. It concluded that ARIMA models, KNN, and LSTM performed better for long-term time prediction windows. Researchers in [11] applied the BorutaShap algorithm to identify the most relevant HRV measures from 43 metrics and designed a light gradient boosting machine (LGBM) model to predict the risk of cardiac arrest in ICU patients. In [12], a model was developed using a deep learning framework with long-term recurrent convolutional networks (LRCN), utilizing a single-channel PPG signal to simultaneously predict physiological parameters such as systolic and diastolic blood pressure and heart rate. Notably, [13] summarized nonlinear methods for time series features of HRV, including mathematical methods based on chaos theory, fractal theory, and information methods based on entropy theory. Although these methods have not been widely used in clinical practice, their potential is promising.

The two most classic models in time series analysis are the Autoregressive Integrated Moving Average (ARIMA) model and the Generalized Autoregressive Conditional Heteroskedasticity (GARCH) model. The former is used to predict data trends under the premise of exploring good input data, while the latter captures data fluctuations under heteroskedastic conditions. Both models have their unique focuses and are widely used. In the scholarly work [14], an ARIMA model was employed to generate prognostications for the equity prices of a subset of pharmaceutical firms listed within the NIFTY100 index of the Bombay Stock Exchange. The study detailed in [15] advanced this approach by integrating ARIMA with an SVM in a hybrid schema to forecast the daily and cumulative financial revenue of select Colombian enterprises, leveraging SVM to

rectify the ARIMA model's insufficiencies in capturing nonlinearities within the dataset. In reference [16], the GARCH (1, 1) model was applied to predict stock price trends on the Indonesia Stock Exchange. Reference [17] employed the GARCH- MIDAS framework to examine the interplay between climatic variations and the volatility of fossil fuel prices.

3. Optimized Hybrid ARIMA-GARCH Model

3.1 Data Features and Data Processing

HRV data inherently exhibits high volatility, statistically expressing as non-stationarity, heteroscedasticity, and left-skewed distribution. The paper employs relevant tests and visualization methods to address these factors and demonstrate their properties. Furthermore, the one-sided Hodrick Prescott (HP-1s) filter is utilized to decompose the data, thereby incorporating these factors and significantly enhancing the accuracy of predictions. The technical details of the process are as follows.

3.1.1 One-sided Hodrick Prescott Filter

For the given HRV data, the original plan was to employ the two-sided Hodrick Prescott (HP-2s) filter to decompose the raw data into the trend component by solving an optimization problem, as shown in Formula (1) [18]. Here, t denotes the time of the sample points, y_s denotes the raw data, τ_s denotes the trend component, and λ denotes the parameter that controls the degree of smoothness of the trend component.

$$\arg\min_{\tau_1,\ldots,\tau_t}\left(\sum_{s=1}^{T}\left(y_s-\tau_s\right)^2+\lambda\sum_{s=2}^{T-1}\left(\tau_{s+1}-2\tau_s+\tau_{s-1}\right)^2\right) \tag{1}$$

However, as observed from Formula (1), the calculation of the trend component at each time point depends partially on future information, which significantly affects the feasibility of the model. The paper introduces the one-sided Hodrick Prescott (HP-1s) filter to address this issue. In contrast, the HP-1s filter calculates the trend component at each time point based solely on current and past information, making it suitable for data prediction, as shown in Formula (2). Here, t denotes the time of the sample points, y_s denotes the raw data, τ_s denotes the trend component, and λ denotes the parameter that controls the degree of smoothness of the trend component, with a typical model selection of $\lambda = 650$ [18].

$$\arg\min_{\tau_t}\left(\min_{\tau_1,\ldots,\tau_{t-1}}\left(\sum_{s=1}^{t}\left(y_s-\tau_s\right)^2+\lambda\sum_{s=2}^{t-1}?\left(\tau_{s+1}-2\tau_s+\tau_{s-1}\right)^2\right)\right) \tag{2}$$

(2) The HP-1s filter is a linear moving average filter. Consequently, the raw data can be expressed as a linear combination of the trend and cycle components, as shown in Formula (3). Here, y_t denotes the raw data, τ_t denotes the trend component, and ψ_t denotes the cycle component [18].

$$y_t = \tau_t + \psi_t \tag{3}$$

3.1.2 Non-stationarity and Heteroscedasticity

Non-stationarity depicts the condition in which the mean, variance, or autocovariance of a time series changes over time, while heteroscedasticity describes the situation where the variance of the error terms in a time series is not constant. Given the high volatility of HRV data, the characteristics of non-stationarity and heteroscedasticity can be directly inferred from the observation of line charts of the raw data and residuals, respectively. Specifically, the experiment selects two portions of the raw data plot and the residual plot and compares the mean, amplitude, and period between the former and latter parts to verify the presence of non-stationarity and heteroscedasticity. This approach is inspired by the core principle of the Goldfeld-Quandt test. To revise the non-stationarity and heteroscedasticity of the raw data, the experimental dataset is designed to undergo a natural logarithmic transformation.

3.1.3 Left-skewed Distribution

The normal distribution is commonly used as a standard for comparing the characteristics of continuous probability distributions. Compared to the Gaussian distribution curve, the peak value of the given HRV data distribution is approximately equal. However, the rate at which the given data distribution curve rises is slower, indicating the probability of minimal values occurring in the raw data is higher. The paper employs the Jarque-Bera normality test to analyze this property, as shown in Formula (4). Here, N denotes the sample size, S denotes the skewness of the distribution, and K denotes the kurtosis of the distribution.

$$JB = \frac{N}{6}\left(S^2+\frac{(K-3)^2}{4}\right) \tag{4}$$

Under the principles of this test, the normal distribution is characterized by a kurtosis of 3 and a skewness of 0. The distribution of the HRV data exhibits a kurtosis close to 3 and a negative skewness, which indicates the left-skewed distribution. Quantile-quantile (Q-Q) plots are constructed for the data to render this analytical outcome visually

apparent. The plot facilitates a comparison between the quantiles of the data and the corresponding normal distribution, thereby assessing the conformity of the data to the normal distribution. The discrepancies between the left-skewed and normal distributions are identified by examining the deviation of points from the diagonal line in the Q-Q plot.

3.2 Partitioning-Interpolation Techniques

After extracting the cycle component using the HP-1s filter, the data cannot be directly used for backward prediction in the GARCH model. Due to the high volatility of the cycle component, it contains not only a majority of valid data but also includes outliers, error terms, or disturbance terms. Therefore, this paper introduces partitioning-interpolation techniques with the aim of identifying a GARCH model of global significance to achieve optimal accuracy.

3.2.1 Partitioning

The principle of partitioning is relatively straightforward. The original cycle component can be regarded as a sequence of sample points, as shown in Formula (5). Here, c_T denotes the last sample point of the cycle component.

$$C = \{c_1, c_2, \cdots, c_T\} \tag{5}$$

The sampling step size is defined as S, and the original sample sequence can be equally divided into S partitions, as shown in Formula (6) [8]. Apparently, each partition contains T / S sample points.

$$PC1, PC2, \cdots, PCS = \{c_1, c_{S+1}, c_{2S+1}, \cdots\}, \{c_2, c_{S+2}, c_{2S+2}, \cdots\}, \cdots, \{c_S, c_{2S}, c_{3S}, \cdots\} \tag{6}$$

Afterward, the paper employs linear interpolation techniques to supplement the number of sample points in each partition to match the original sample sequence, resulting in each partition containing T sample points.

3.2.2 Sampling Step Size

The selection of the sampling step size is not arbitrary. An excessively large one may result in partitions that fail to capture consecutive important information within the original sample sequence, while a tiny one may lead to the partitioning technique losing its effectiveness in extracting valid information. According to the Nyquist sampling theorem, the sampling frequency should be at least twice the signal's highest frequency [19]. To determine the sampling step size, it is necessary first to determine the signal's highest frequency. The paper introduces the Fast Discrete Fourier Transform (FDFT) to convert the discrete sample sequence into a continuous signal, as shown in Formula (7). Here, $f_N(k)$ denotes the transformed complex frequency-domain sequence, N denotes the sample size, c_n denotes the original time-domain signal sequence, and j denotes the imaginary unit.

$$f_N(k) = \sum_{n=0}^{N-1} c_n e^{jn\frac{2\pi}{N}k} \tag{7}$$

Once the continuous signal is obtained, the experiment identifies the signal's highest frequency by plotting spectral diagrams and observing the highest frequency in the spectrum.

4. Experimental Procedure and Result Analysis

4.1 Experimental Steps

The experiment employs the long-term RR interval time series from 147 volunteers, ranging in age from 1 month to 55 years, who have not undergone pharmacological treatment and exhibit regular ECG readings. The University of La Plata, Argentina, shared the dataset. It was made available through the Research Resource for Complex Physiologic Signals website, managed by the Computational Physiology Laboratory at MIT. The data from three test subjects, No. 000, No. 410, and No. 4100, are chosen for presentation. Subject No. 000 is a 53-year-old male, subject No. 410 is a 12-year-old female, and subject No. 4100 is a one-month-old male infant [5, 6, 7]. The purpose of the experiment is to utilize these three sets of differentiated individual data to reflect the optimized hybrid ARIMA-GARCH model's excellent predictive accuracy and generalization capabilities. The detailed experimental steps are as follows.

1) The raw HRV data are naturally logarithmically transformed and then input into the HP-1s filter, decomposed into a sum of a trend component with low volatility and high trend and a cycle component with high volatility and low trend.

2) The trend component is divided into training sets and testing sets. The ARIMA (p, d, q) model is directly applied to predict the trend component after determining the order using a grid search method, obtaining the predictions for the following ten periods of the trend component.

3) The cycle component is transformed into a continuous signal through the FDFT, and spectral diagrams are plotted to observe the highest frequency. Then, according to the Nyquist theorem, the sampling step size is calculated.

4) With the obtained sampling step size, the cycle component sequence is equally divided into several partitions and linear interpolation is used to complete the sampling points for each partition.

5) Each completed partition is input into the GARCH (1, 1) model separately, and the evaluation metrics are

calculated to ascertain the optimal GARCH model. The experiment selects the GARCH (1, 1) model with the best accuracy for global cycle component prediction, obtaining the predictions for the following ten periods of the cycle component.

6) The experiment sums the predictions of the following ten periods of the trend component and the following ten periods of the cycle component to obtain the predicted data for the following ten periods.

7) The predicted data for the following ten periods are reverted to predicted HRV data via a natural exponential transformation.

4.2 Data Analysis

4.2.1 Analysis of the Data Decomposition

The experiment separately generates three groups of graphs for test subject No. 4100 as an example, depicting the natural logarithm-transformed HRV data, the trend component, and the cycle component. Each group of graphs includes the following three types.

Ø A line chart of the first one thousand sample points of the data.

Ø A residual plot of the first one thousand sample points of the data.

Ø A Q-Q plot compares the data's left-skewed distribution to the corresponding normal distribution.

As shown in Figure 1, the first row of graphs verifies the non-stationarity, heteroscedasticity, and left-skewed distribution of the raw data. The second and third rows of graphs demonstrate that the experiment successfully decomposes the raw data into a linear part with high trend and low volatility, which satisfies the Gauss-Markov assumption, and a nonlinear part with low trend and high volatility. It provides a theoretical basis for the proposed model.

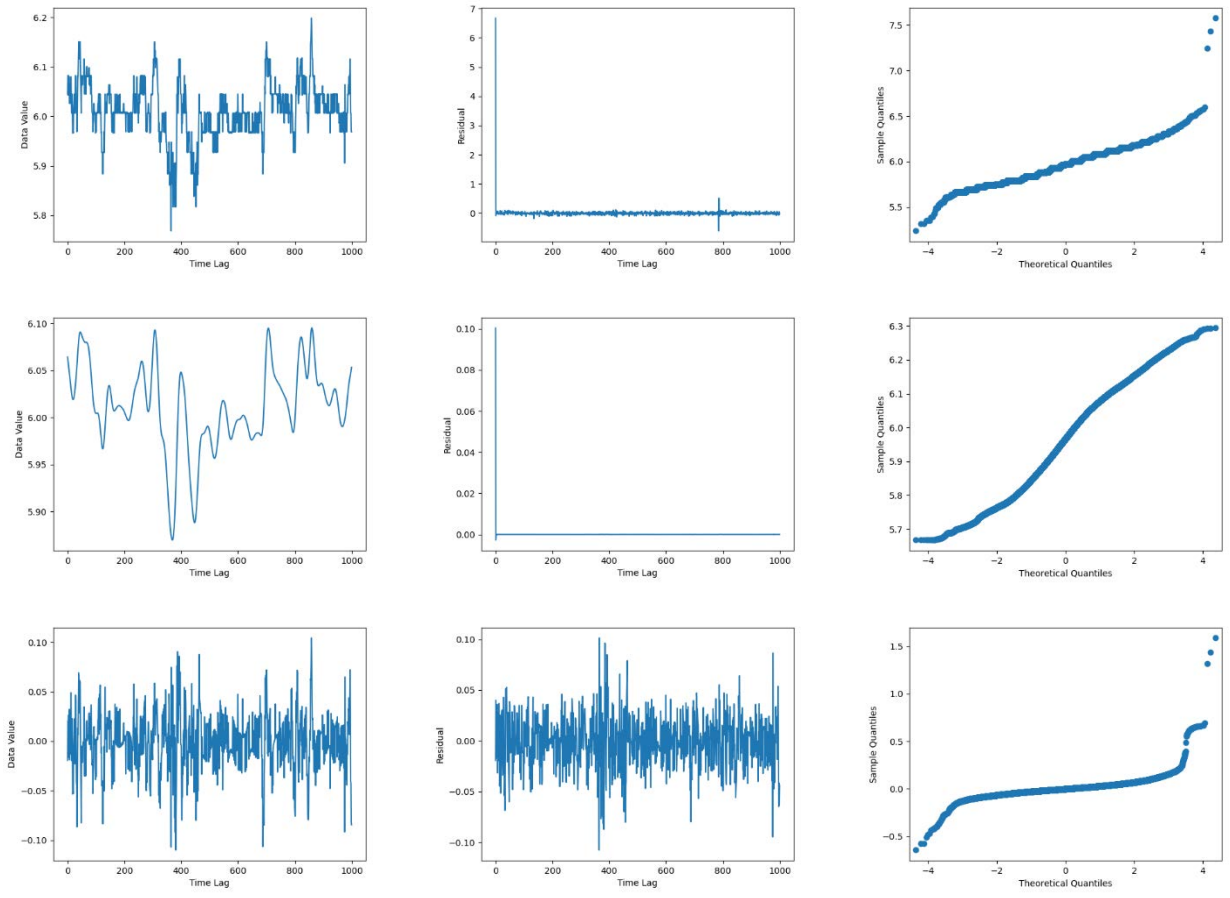

Figure 1 Data features of the raw data, the trend component and the cycle component

4.2.2 Analysis of the Sampling Step Size

The experiment plots the spectral diagrams of the continuous signals generated by the fast discrete Fourier transform of the cycle components for three test subjects, No. 000, No. 410, and No. 4100, as shown in Figure 2. The experiment adopts the maximum integer sampling step

size within the feasible sampling step size interval. It constructs a table to display the highest frequency of each cycle component and the corresponding sampling step size. As shown in Table 1, the cycle component for test subject No. 000 is divided into 10 partitions, the cycle component for test subject No. 410 is divided into 14 partitions, and the cycle component for test subject No. 4100 is divided into 15 partitions.

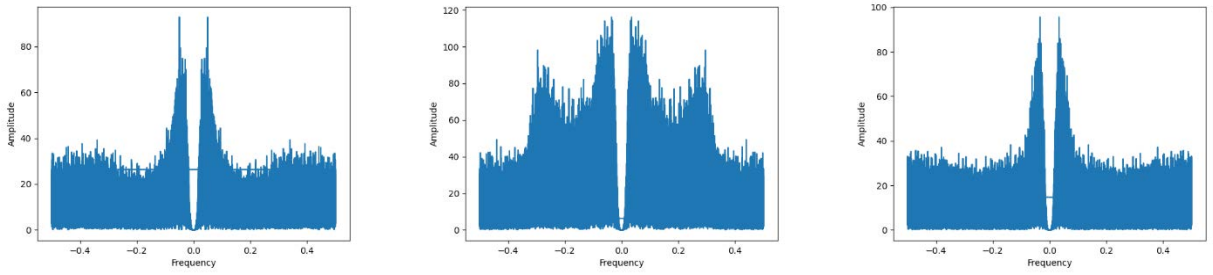

Figure 2 Spectral diagram of No. 000, No. 410 and No. 4100

Table 1 Highest frequency and sampling step size observed in spectrum

Number	Highest Frequency (HZ)	Sampling Step Size
No. 000	0.0500	10
No. 410	0.0353	14
No. 4100	0.0333	15

4.3 Experimental Results

The experiment utilizes the HRV datasets from three test subjects, No. 000, No. 410, and No. 4100. It not only evaluates the predictive performance of the proposed optimized hybrid ARIMA-GARCH model but also examines the forecasting powers of the standalone ARIMA model and machine learning techniques, including SVM and Random Forests. Guided by a suite of following evaluation criteria, the research substantiates the superior data prediction and generalization capabilities of the model introduced in this paper.

The Mean Squared Error (MSE) computes the average of the squared differences between the predicted values and actual values, as shown in Formula (8). Here, n denotes the sample size, Y_i denotes the actual values of the sample points, and $\hat{Y}_i$ denotes the corresponding predicted values. MSE is more sensitive to more significant discrepancies between predicted and actual values. Moreover, a smaller MSE indicates a higher prediction accuracy of the model.

$$MSE = \frac{1}{n}\sum_{i=1}^{n}?\left(Y_i - \hat{Y}_i\right)^2 \tag{8}$$

The Mean Absolute Error (MAE) directly computes the average of the differences between the predicted values and actual values, as shown in Formula (9). Here, n denotes the sample size, Y_i denotes the actual values of the sample points, and $\hat{Y}_i$ denotes the corresponding predicted values. MAE intuitively measures the absolute difference between each pair of predicted values and actual values. Moreover, a smaller MAE suggests a higher model prediction accuracy.

$$MAE = \frac{1}{n}\sum_{i=1}^{n}?\left|Y_i - \hat{Y}_i\right| \tag{9}$$

The Mean Absolute Percentage Error (MAPE) computes the average proportion of the absolute difference between the predicted and actual values to the actual values, as shown in Formula (10). Here, n denotes the sample size, Y_i denotes the actual values of the sample points, and $\hat{Y}_i$ denotes the corresponding predicted values. MAPE provides a percentage perspective. Moreover, a smaller MAPE indicates a higher prediction accuracy of the model.

$$MAPE = \frac{1}{n}\sum_{i=1}^{n}?\left|\frac{Y_i - \hat{Y}_i}{Y_i}\right| \times 100\% \tag{10}$$

As shown in Table 2, Table 3, Table 4, all three groups of models fully reveal the dominance of the proposed model over other models, particularly in the realm of time series prediction. Compared to machine learning models, the proposed model shows approximately a 14% ~ 65% improvement in MSE, a 5% ~ 33% improvement in MAE, and an 8% ~ 25% improvement in MAPE. Against time series forecasting models, our model exhibits roughly a 36% ~ 1020% improvement in MSE, a 35% ~ 385% im-

provement in MAE, and a 28% ~ 357% improvement in MAPE. The nonlinear components within the HRV data account for the substantial discrepancies in the model performances.

Table 2 Model performance of test subject No. 000

Model	MSE	MAE	MAPE (100%)
Proposed Model	1429.3576	27.6805	4.3663
ARIMA	2503.2209	42.8835	6.3191
SVM	1631.4795	36.6637	5.4956
Random Forest	1655.9440	33.0340	4.9355

Table 3 Model performance of test subject No. 410

Model	MSE	MAE	MAPE (100%)
Proposed Model	802.0422	20.7585	3.5113
ARIMA	1091.2436	27.8903	4.5475
SVM	1050.6476	23.3536	3.8916
Random Forest	984.7350	21.2500	3.5799

Table 4 Model performance of test subject No. 4100

Model	MSE	MAE	MAPE (100%)
Proposed Model	84.2624	7.7471	2.1034
ARIMA	857.5100	27.4977	7.5019
SVM	116.5903	9.1454	2.4741
Random Forest	139.9550	7.8500	2.1156

5. Conclusion

In this paper, an improved model is proposed based on the hybrid ARIMA-GARCH framework by incorporating the HP-1s filter, partitioning-interpolation technique, and FDFT. The purposed model offers novel insights and a scientific foundation for the advancement of both cardiovascular disease prevention and treatment, as well as the improvement of medical devices. The experiment utilizes the RR interval time series data with high volatility as the testing dataset. MSE, MAE, and MAPE are computed for the proposed model and compared with the ARIMA model, SVM, and random forest to demonstrate the high accuracy and generalization capability in short-term forward prediction. The paper also acknowledges that the data distribution can be further optimized to achieve better prediction accuracy, and the model exhibits deficiencies in long-term forecasting. These aspects are identified as future directions for research.

References

[1] Oyeleye, M., Chen, T., Titarenko, S., & Antoniou, G., A Predictive Analysis of Heart Rates Using Machine Learning Techniques, International Journal of Environmental Research and Public Health, 19(4), 2417, 2022.

[2] Alharbi, A., Alosaimi, W., Sahal, R., & Saleh, H., Real-time System Prediction for Heart Rate Using Deep Learning and Stream Processing Platforms, Complexity, 2021, 1-9.

[3] Hinde, K., White, G., & Armstrong, N., Wearable Devices Suitable for Monitoring Twenty Four Hour Heart Rate Variability in Military Populations, Sensors, 21(4), 1061, 2021.

[4] The, A. F., Reijmerink, I., van der Laan, M., & Cnossen, F., Heart Rate Variability as a Measure of Mental Stress in Surgery: A Systematic Review, International Archives of Occupational and Environmental Health, 93, 805-821, 2020.

[5] Irurzun, I. M., Garavaglia, L., Defeo, M. M., & Thomas Mailland, J., RR Interval Time Series from Healthy Subjects (Version 1.0.0), PhysioNet, 2021.

[6] Garavaglia, L., Gulich, D., Defeo, M. M., Mailland, J. T.,

Irurzun, I. M., The Effect of Age on the Heart Rate Variability of Healthy Subjects, Plos One.

[7] Goldberger, A., Amaral, L., Glass, L., Hausdorff, J., Ivanov, P. C., Mark, R., ... & Stanley, H. E., PhysioBank, PhysioToolkit, and PhysioNet: Components of a New Research Resource for Complex Physiologic Signals. Circulation [Online]. 101 (23), 2000, pp. e215-e220.

[8] Babu, C. N., & Reddy, B. E., Prediction of Selected Indian Stock Using a Partitioning-interpolation Based ARIMA-GARCH Model, Applied Computing and Informatics, 11(2), 2015, 130-143.

[9] Ding, C., Duan, J., Zhang, Y., Wu, X., & Yu, G., Using an ARIMA-GARCH Modeling Approach to Improve Subway Short-term Ridership Forecasting Accounting for Dynamic Volatility, IEEE Transactions on Intelligent Transportation Systems, 19(4), 2017, 1054-1064.

[10] Dritsaki, C., The Performance of Hybrid ARIMA-GARCH Modeling and Forecasting Oil Price, International Journal of Energy Economics and Policy, 8(3), 2018, 14-21.

[11] Lee, H., Yang, H. L., Ryu, H. G., Jung, C. W., Cho, Y. J., Yoon, S. B., ... & Lee, H. C., Real-time Machine Learning Model to Predict In-hospital Cardiac Arrest Using Heart Rate Variability in ICU, NPJ Digital Medicine, 6(1), 215, 2023.

[12] Panwar, M., Gautam, A., Biswas, D., & Acharyya, A., PP-Net: A Deep Learning Framework for PPG-based Blood Pressure and Heart Rate Estimation, IEEE Sensors Journal, 20(17), 2020, 10000-10011.

[13] Henriques, T., Ribeiro, M., Teixeira, A., Castro, L., Antunes, L., & Costa-Santos, C., Nonlinear Methods Most Applied to Heart-rate Time Series: A Review, Entropy, 22(3), 309, 2020.

[14] Meher, B. K., Hawaldar, I. T., Spulbar, C. M., & Birau, F. R., Forecasting Stock Market Prices Using Mixed ARIMA Model: A Case Study of Indian Pharmaceutical Companies, Investment Management and Financial Innovations, 18(1), 2021, 42-54.

[15] Rubio, L., & Alba, K., Forecasting Selected Colombian Shares Using a Hybrid ARIMA-SVR Model, Mathematics, 10(13), 2181, 2022.

[16] Endri, E., Abidin, Z., Simanjuntak, T. P., & Nurhayati, I., Indonesian Stock Market Volatility: GARCH Model, Montenegrin Journal of Economics, 16(2), 2020, 7-17.

[17] Tumala, M. M., Salisu, A., & Nmadu, Y. B., Climate Change and Fossil Fuel Prices: A GARCH-MIDAS Analysis, Energy Economics, 124, 106792, 2023.

[18] Wolf, E., Mokinski, F., & Schüler, Y. S., On Adjusting the One-sided Hodrick-Prescott Filter, Available at SSRN 3536248, 2020.

[19] Lathi, B. P., & Green, R. A., Signal Processing and Linear Systems (Vol. 2), Oxford: Oxford University Press, 1998.